

The interaction of droplet dynamics and turbulence cascade

Original

The interaction of droplet dynamics and turbulence cascade / Crialesi-Esposito, Marco; Chibbaro, Sergio; Brandt, Luca. - In: COMMUNICATIONS PHYSICS. - ISSN 2399-3650. - 6:1(2023). [10.1038/s42005-022-01122-8]

Availability:

This version is available at: 11583/2990229 since: 2024-07-02T14:20:36Z

Publisher:

NATURE PORTFOLIO

Published

DOI:10.1038/s42005-022-01122-8

Terms of use:

This article is made available under terms and conditions as specified in the corresponding bibliographic description in the repository

Publisher copyright

Springer postprint/Author's Accepted Manuscript

This version of the article has been accepted for publication, after peer review (when applicable) and is subject to Springer Nature's AM terms of use, but is not the Version of Record and does not reflect post-acceptance improvements, or any corrections. The Version of Record is available online at: <http://dx.doi.org/10.1038/s42005-022-01122-8>

(Article begins on next page)

The interaction of droplet dynamics and turbulence cascade

Marco Cialesi-Esposito ^{1,2}✉, Sergio Chibbaro ^{3,4}✉ & Luca Brandt ^{1,5}✉

The dynamics of droplet fragmentation in turbulence is described by the Kolmogorov-Hinze framework. Yet, a quantitative theory is lacking at higher concentrations when strong interactions between the phases and coalescence become relevant, which is common in most flows. Here, we address this issue through a fully-coupled numerical study of the droplet dynamics in a turbulent flow at $R_\lambda \approx 140$, the highest attained up to now. By means of time-space spectral statistics, not currently accessible to experiments, we demonstrate that the characteristic scale of the process, the Hinze scale, can be precisely identified as the scale at which the net energy exchange due to capillarity is zero. Droplets larger than this scale preferentially break up absorbing energy from the flow; smaller droplets, instead, undergo rapid oscillations and tend to coalesce releasing energy to the flow. Further, we link the droplet-size distribution with the probability distribution of the turbulent dissipation. This shows that key in the fragmentation process is the local flux of energy which dominates the process at large scales, vindicating its locality.

¹FLOW, Department of Engineering Mechanics, KTH Royal Institute of Technology, Stockholm, Sweden. ²INFN, Sezione di Torino, Via Pietro Giuria 1, 10125 Torino, Italy. ³Université Paris-Saclay, CNRS, LISN, 91400 Orsay, France. ⁴SPEC, CEA, CNRS UMR 3680, Université Paris-Saclay, CEA Saclay, Gif-sur-Yvette, France. ⁵Department of Energy and Process Engineering, Norwegian University of Science and Technology (NTNU), Trondheim, Norway.
✉email: crialesi@to.infn.it; sergio.chibbaro@upsaclay.fr; luca@mech.kth.se

Turbulent flows with dispersed interfaces are at the core of many transfer processes in gas-liquid (atomization and sprays)^{1–3} and liquid-liquid (emulsions) systems^{4–6}. Notably, air bubbles are key for the gas transfer between ocean and atmosphere^{7–9}, and in the aerosol production through bursting^{10,11}. Despite the numerous experimental and numerical studies^{12–17}, the nature of the interactions between droplets of different sizes and turbulence is not yet clear. The presence of a deforming/breaking/coalescing interface couples the two phases in a non-trivial way, absorbing and distributing energy over the whole spectrum of scales. The Kolmogorov-Hinze (KH) theory^{18,19} is the cornerstone of existing models and applications; this framework is based on the breakup of isolated droplets in turbulence and identifies the scale d_H above which a droplet breaks up due to the local environment turbulence and below which surface tension forces are able to resist the action of the turbulent eddies. This picture, based on breakup only, is incomplete and has been recently challenged²⁰.

The key observable is the distribution spectrum of the size of the intrusions, $\mathcal{N}(d)$, which gives the number of droplet at a given size d . The dynamics for large diameters has been rationalized in the KH framework in terms of a local fragmentation process⁷. The idea is that a droplet breaks up whenever the pressure forces acting on its surface are larger than the cohesive force given by the surface tension. In this picture, the only dimensionless parameter is the Weber number $We = \rho_c u_d^2 d / \sigma$, where ρ_c is the carrier-phase density, σ is the surface tension, and u_d is the typical velocity at the scale of the droplet size, d . The disruptive inertial-range velocity fluctuations can initiate fragmentation above a critical threshold We_c ²¹. Assuming the local Kolmogorov description of turbulence in the inertial range^{7,22}, $u_d^2 \sim \langle \varepsilon \rangle^{2/3} d^{2/3}$, where $\langle \varepsilon \rangle = \langle \nu(\partial_i u_j + \partial_j u_i)^2 \rangle$ is the time-space average energy dissipation rate, and using dimensional analysis, Kolmogorov and Hinze first derived an estimate for the maximum droplet size for which surface tension is able to resist the pressure fluctuations^{7,18,19}:

$$d_H = \left(\frac{We_c}{2} \right)^{3/5} \left(\frac{\rho_c}{\sigma} \right)^{-3/5} \langle \varepsilon \rangle^{-2/5}. \quad (1)$$

This is referred to as the Hinze scale, and it is the only length scale that can be obtained from $\rho_c, \sigma, \langle \varepsilon \rangle$. For $d \gtrsim d_H$ surface tension forces cannot resist pressure fluctuations, and the droplets break. A fragmentation cascade is thus triggered, with a power-law size distribution $\mathcal{N}(d) \sim d^{-10/3}$ obtained by dimensional analysis solely assuming locality⁷, see also Supplementary Note 1 for details. Empirical evidences, notably in bubbly flows, seem to confirm this distribution^{7,9,23–26}, although variations may be measured, in particular because of viscous effects in emulsions²⁷. Yet, recent experiments on a single bubble contradict this physical picture²⁰, and the definition of the critical Weber number We_c remains ambiguous and somewhat heuristic, with values in the literature spanning more than one order of magnitude^{16,23,28}. Furthermore, the key feature of intermittency, that is the breaking of scale invariance^{29–31}, has not been considered in the analysis.

Even less clear is the behavior for $d \lesssim d_H$, where observations seem to indicate a different power-law spectrum $\mathcal{N}(d) \sim d^{-3/29,23}$; laboratory experiments are difficult and no fundamental study of the collective turbulent dynamics of droplets or bubbles is currently available.

To overcome these difficulties and fully understand the problem by gaining access to quantities difficult to measure in the laboratory, we carry out a large campaign of direct numerical simulations (DNS) of turbulent multiphase flows. The simulations are performed at a high-level of multiphase turbulence, $Re_\lambda \approx 137$, varying the surface tension, volume fraction α , and the

ratio of the two fluid viscosity. Key to our understanding is the scale-by-scale energy budget, accessible only in numerical experiments (See Material and Methods for the details on the theoretical tools and the setup employed). In this work, we provide a comprehensive explanation by considering configurations in which turbulence is modulated by the dispersed phase and both coalescence and breakup occur. We will use an original statistical approach analyzing the energy fluxes from fully resolved numerical simulations to unambiguously show that there exists a scale d_H which separates two regimes—one statistically dominated by non-local processes, like droplet coalescence, and the other by breakup. We also show that intermittency at small scales significantly increases in multiphase turbulence and demonstrate how the extreme-event distribution can be inferred directly by the droplet size distribution.

Results

Scale interpretation of droplet size spectrum. Figure 1(a) shows a visualization of the mixture for a volume fraction of the dispersed phase $\alpha = 0.1$ and viscosity ratio 1. The dispersed phase, initially a single droplet, is organizing over different scales and shapes, from large-scale drops to smaller filaments and even smaller droplets. The droplet size distribution is shown for different volume fractions in the main panel of Fig. 1 with the two scaling regimes introduced above emphasized in the inset (b). The small-scale range is similar for the different cases, whereas the large-scale distribution is sensitive to changes in the volume fraction. At large volume fractions, nevertheless, our results fully support the two empirically-proposed laws, remarkably neatly for $\alpha = 0.5$. For small volume fractions of the dispersed phase, instead, the spectrum appears to fall exponentially at large scales. Furthermore, the distribution spectra are only slightly altered when changing the viscosity, as shown by the collapse of the data at fixed volume fraction in panel (b).

The cross-over scale separating the two power-laws is the Hinze scale, and is usually determined from the value of We_c . In Fig. 2(a), we show $C = (We_c/2)^{3/5}$ as the iso-lines interpolating all simulated conditions as a function of the two dimensionless groups $\rho_c \sigma D_{95} / \mu_c^2$ and $\mu_c^4 \varepsilon / \rho_c \sigma^4$, where D_{95} is the diameter for which 95% of the total mass is enclosed in droplets smaller than D_{95} , a measure of the maximum diameter at which a droplet breaks at We_c ¹⁹. Our results confirm that a unique value of the coefficient C cannot be used to fit all the data. In particular, when surface tension is varied while taking the viscosity of the two fluids equal, data nicely collapse on a line of slope $C \approx 1$. However, increasing μ_d / μ_c and α , while maintaining the dissipation $\langle \varepsilon \rangle$ almost constant, C should be increased to about 2.5 to fit the data. Note that the range $C \in [1, 2.5]$ corresponds to a critical Weber number in the range $2 < We_c < 9.5$; with even larger deviations observed in literature¹⁶. This variability of We_c limits the applicability of the original definition of the Hinze scale.

We can however provide an accurate calculation of the cross-over scale by analyzing the scale-by-scale energy fluxes^{32,33}, which written in Fourier space read (see Material and Methods):

$$\partial_t \mathcal{E}(\kappa) = T(\kappa) + \mathcal{D}(\kappa) + \mathcal{S}_\sigma(\kappa) + \mathcal{F}(\kappa), \quad (2)$$

where $\mathcal{E}(\kappa)$ is the energy spectrum, $T(\kappa)$ the energy transfer due to the nonlinear term, $\mathcal{D}(\kappa)$ the viscous dissipation, $\mathcal{S}_\sigma(\kappa)$ the work of the surface tension force, and $\mathcal{F}(\kappa)$ is the power injected by the forcing used to maintain the turbulence. In Fig. 2(b), we display the net transfer due to the action of surface tension forces and the droplet size distribution versus the wavenumber κ . The comparison of the scale-by-scale budget and the size-distribution clearly points out that the cross-over scale is

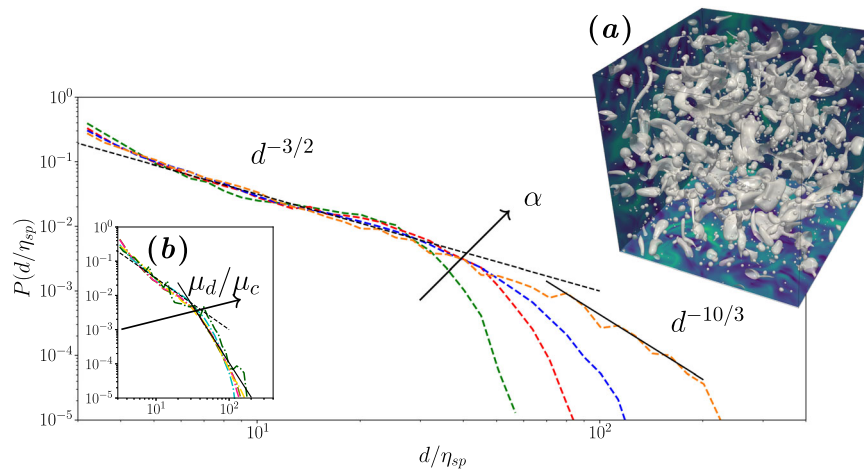


Fig. 1 The droplet-size-distribution of emulsions in homogeneous and isotropic turbulence. Droplet-size-distribution for emulsions in homogeneous and isotropic turbulence at different volume fractions α , i.e., 0.03 (green dashed line) 0.06 (red dashed line) 0.1 (blue dashed line) 0.5 (ocher dashed line) at constant large-scale Weber number (see Methods) $We_L = 42.6$ and $\mu_d/\mu_c = 1$. The droplet diameter is normalized with the Kolmogorov scale η_{sp} for the single-phase reference case (also used as initial condition for all simulations) at $Re_L = 137$. Similarly, inset (b) shows the DSD different viscosity ratio μ_d/μ_c , i.e., 0.01 (black dot-dashed line) 0.1 (red dot-dashed line) 1 (cyan dot-dashed line) 10 (yellow dot-dashed line) 100 (dark green dot-dashed line), at constant $\alpha = 0.1$ and $We_L = 42.6$. The black dashed line indicates the $-3/2$ power-law and the continuous black line the $-10/3$ power-law. Inset (a) shows a render of the simulation at $We_L = 42.6$, $\alpha = 0.1$ and $\mu_d/\mu_c = 1$. The droplets diameter is considered to be the volumetric one, i.e., $d = (6V_d/\pi)^{1/3}$, with V_d the droplet volume.

unambiguously defined as the length at which the work made by surface tension is zero, called hereafter as $d_{H\sigma}$. It is found that this is generally different from the standard d_H computed through (1).

At larger scales (small κ), $S_\sigma(\kappa) < 0$ which implies drainage by the surface tension forces. This indicates that, at these scales, cohesive forces are not able to resist disruptive turbulent eddies and we should expect fragmentation to dominate. In this regime, assuming statistical scale locality, that is droplets are broken only by eddies of comparable size, it is possible to obtain the $-10/3$ power-law for the droplet-size-distribution⁷. As in all turbulent cascades³⁴, the local picture cannot be strictly true. Indeed, since droplets are stable due to surface tension when $d < d_{H\sigma}$ the local cascade would induce an accumulation of droplets at $\ell \approx d_{H\sigma}$ and no smaller ones, at least in a statistical sense. We therefore expect this picture to be accurate only for $d \gtrsim d_{H\sigma}$ and a non-local process to determine large-scale events. In fact, two similar daughter drops and some smaller droplets form as a result of the breakup of large droplets, $d \gg d_{H\sigma}$ as confirmed experimentally^{26,35}. It is worth emphasizing that the droplet-cascade process can be still approximated as local, since small droplets have negligible volume. Yet, non-local effects are necessary to explain the existence of droplets with $d < d_{H\sigma}$.

At small scales, droplets cannot break up as the surface tension is larger than the dynamic pressure, rather they should coalesce for they try to minimize the free energy, that is the surface area. In this case, we find positive work made by surface tension forces, that is interface deformation increases the flow kinetic energy, rather than absorbing it as at large scales; this is shown by the rightmost part of the spectrum in Fig. 2(b). The full scale-by-scale global budgets is shown in Supplementary Fig. 1 and further discussed in ref. ³⁶. It is important to note that the turbulence cascade is not necessarily intended here to be related to a constant non-linear flux from large to small scales, because of the contribution of the surface tension.

For geometric reasons, it is more likely to have collisions and coalescence between small and large droplets³⁷, which promotes the non-locality of the inverse droplet-cascade. The introduction of a second large-scale other than the droplet diameter allows to retrieve the $-3/2$ scaling^{7,23}, see SI. The closer the droplets are to

the Hinze scale from below, i.e., $d \lesssim d_{H\sigma}$, the more local is the process, and droplets of similar size are more likely to interact. For $d = d_{H\sigma}$ both mechanisms occur and the net energy transfer from surface tension is thus exactly zero i.e., $S_\sigma(\kappa_{S_\sigma}) = 0$, with $\kappa_{S_\sigma} = 2\pi/d_{H\sigma}$. At this scale, we observe the transition between the $-10/3$ and the $-3/2$ power-laws. The non-locality and randomness of the coalescence events suggest that this process is not likely the only source for positive surface tension work at small scales. In fact, random coalescence events should have a considerably high frequency to sustain small scale agitation, which is unlikely at very low volume fractions. One possible production mechanism is the collision between a droplet and vortices of similar size but unable to break the interface, producing velocity fluctuations of scale smaller than the droplet size. A precise estimation of all the mechanisms leading to small-scale agitation is difficult to obtain from statistical data and requires additional ad-hoc numerical experiments. Our physical picture based on energy considerations are to be true in a statistical sense, but we expect it to be qualitatively true also for each single realization. Therefore, in order to gain a better understanding of the small-scale dynamics, we remove the effect of coalescence at statistical steady state from the picture, and study the behavior in wave-number space of a single droplet break up.

Single-droplet breakup. The statistical interpretation of the break-up/coalescence process described so far relies on the assumption that a droplet can be considered as a spherical object, such that local variations of the surface curvature are statistically negligible. Of course, this cannot be true for a single break-up, and one must provide a link between the single-droplet dynamics and the multiphase flow statistics. The morphological analysis of a droplet break-up in turbulence enables us to identify three stages, see Fig. 3: *incipient* deformation (green panels), *sub-critical* deformation (yellow panels) and *super-critical* deformation (red panels). In the *incipient* deformation stage, the droplet, originally spherical, deforms due to the interaction with the turbulence, panel (a). At this stage, the turbulent kinetic energy is mainly absorbed at large and intermediate scales, as shown by the work

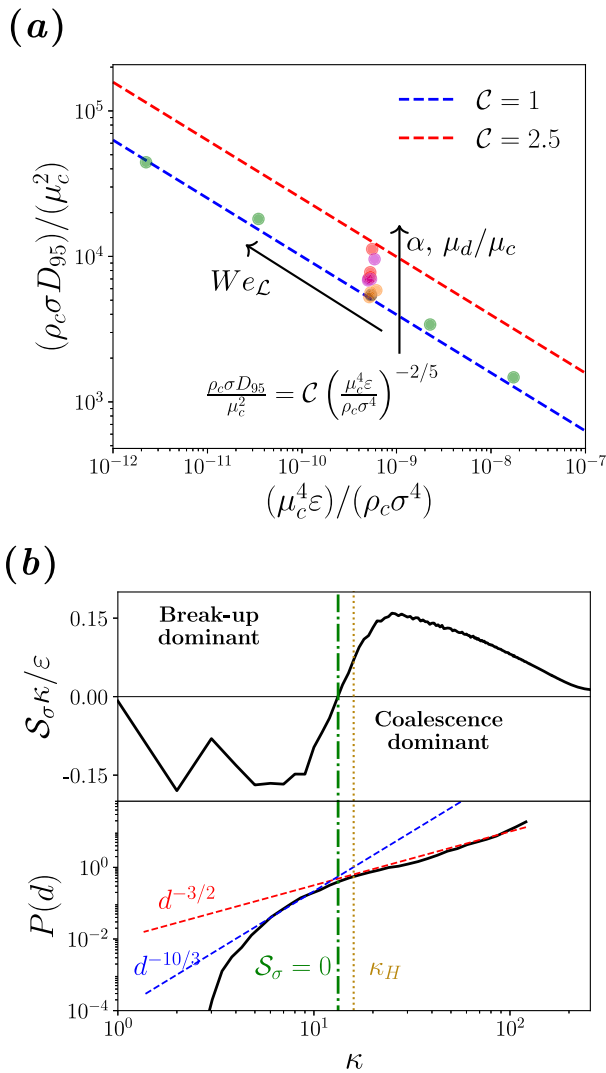


Fig. 2 The definition of the Kolmogorov-Hinze scale. **a** Maximum droplet diameter D_{95} as a function of the energy input ε , normalized as in ref. ¹⁹. We performed several simulations, varying one parameter (i.e., α , μ_d/μ_c and $We_{\mathcal{L}}$) at the time. We show results for different α (red dots) at $We_{\mathcal{L}} = 42.6$ and $\mu_d/\mu_c = 1$; different $We_{\mathcal{L}}$ (green dots) at $\mu_d/\mu_c = 1$ and $\alpha = 0.03$; different μ_d/μ_c (purple dots) at $\alpha = 0.1$ and $We_{\mathcal{L}} = 42.6$, and different μ_d/μ_c (yellow dots) at $\alpha = 0.03$ and $We_{\mathcal{L}} = 42.6$. The arrows indicate data obtained with increasing values of each parameter. The blue line shows $C = (We_{\mathcal{L}}/2)^{3/5} = 1$, whereas $C = 0.765$ was originally proposed¹⁹. **b** The relationship between surface tension energy transfer and droplet-size-distribution. Top panel shows the term S_{σ} from Eq. (2), normalized by the average energy dissipation and multiplied by κ to increase visibility. The bottom panel shows the droplet-size-distribution $P(d)$, versus the wavenumber $\kappa = 2\pi/d$. The vertical lines show $S_{\sigma} = 0$, (green-dashed) and the Hinze scale wavenumber computed using $C = 1$ (gold-dotted).

of the surface tension S_{σ} in the bottom section of panel (a). Deformation increases with time, progressively forming regions with high values of the curvature ξ (panels b,c). At this *sub-critical* stage, work against surface tension is acting to deform larger interfaces while smaller structures are produced for which interfacial forces are greater than turbulent pressure fluctuations. At these small scales, the interface tends to relax to a spherical shape, releasing energy to the surrounding flow (see areas of $S_{\sigma} > 0$ at the bottom of panels b,c). It can be demonstrated that high local values of ξ are directly responsible for high values of S_{σ}

(see Material and Methods). When *super-critical* deformation is reached, the interface breaks and small droplets form, see panels (d,e). Energy is still absorbed for the deformation of large interfaces, while the coalescence of the small droplets minimizes the surface area and adds energy to the flow at small scales (panels d,e). Simulations pleasantly confirm that most of the fragmentation process is local, while sub-Hinze droplets are formed through a non-local dynamics. Droplets at $d < d_H$ are thus characterized by an oscillatory motion, resulting from deformations by small vortices and viscosity and surface-tension driven relaxation. It should be noted that droplet relaxation and coalescence have a similar energy footprint on the flow, as they both add energy at scales $\ell < d$. At the same time, coalescence contributes to the formation of larger drops, thus affecting energy transfer to larger scales, proving to be the source of non-locality from small to large scales.

After a full large-eddy turnover time $\mathcal{T}_{\mathcal{L}}$, the instantaneous energy transfer due to surface tension forces, S_{σ} , approaches the behavior at the statistically stationary state, corroborating the statistical picture obtained when many droplets are considered. This shows that droplet dynamics for sizes $d < d_{H\sigma}$ and local interface deformations at scale $\ell < d_{H\sigma}$ are associated to the transfer of energy to the carrier phase by interfacial forces. Our simulations clearly show that energy spectra of the carrying phase are modulated by the droplets in a way fully consistent with the above physical picture (see Supporting Movie 1).

Intermittency. The argument leading to the definition of the Hinze scale is based on mean turbulence properties, yet turbulence is characterized by fluctuations exhibiting large deviations from the mean values, i.e., intermittency³². The definition of a Hinze scale based on energy fluxes takes implicitly into account intermittency in an average sense, but it does not give any insight on the role of the extreme events on the droplet size distribution. If the turbulence determines the droplet size distribution and the droplets modulate the turbulence, it should be possible to relate the droplet size distribution to the intermittency at the different scales. If this is the case, we would be able to extract information about the turbulence modulation and dissipation rates from the distribution size spectrum, more accessible to experimental measurements.

Using Eq. (1), the probability distributions of d and ε (here intended as the space-local and instantaneous value of dissipation) may be related by $\varepsilon \sim d^{-5/2}$, so to obtain⁷

$$P(\varepsilon) \sim d^{13/2} \mathcal{N}(d). \tag{3}$$

This relation, further discussed in Supplementary Notes 1, implies that small droplets are correlated to high dissipation events (large ε), while large droplets are related to regions of small ε . This is beautifully confirmed in Fig. 4, where we compare the distribution $P(\varepsilon)$, computed according to Eq. (3), with the dissipation distribution extracted from the simulations. The tail of the distribution, i.e., high ε , which corresponds to small scales and the range of diameters for which the droplet distribution scales as $d^{-3/2}$, is accurately described by Eq. (3) for all cases. For small ε , i.e., large d (see inset), Eq. (3) is in general less accurate, yet improving with α (the whole dissipation distribution is reasonably well predicted for $\alpha = 0.5$). Equation (3) has a clear meaning only where a local fragmentation process is present, which in turn should be related to the inertial-range turbulence, and indeed for increasing values of α more droplets are found to have sizes in the inertial range of scales (see Supplementary Fig. 2). Figure 4 also shows that the degree of intermittency is much higher in multiphase flows than in single-phase turbulence, indicating an increase of extreme events at small scales when coalescence is also

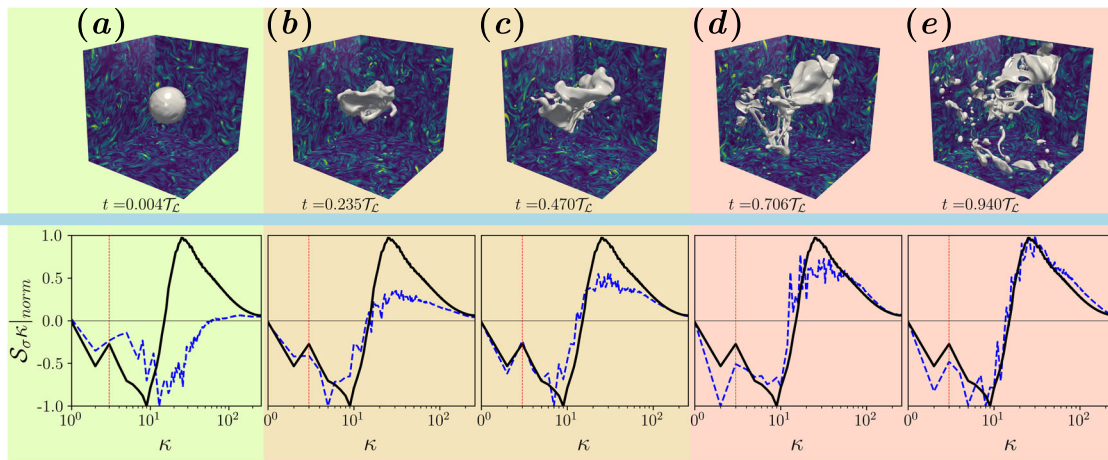


Fig. 3 Time-sequence of a single droplet breakup in turbulence. The simulation is performed at $\mu_d/\mu_c = 1$ and $We_L = 42.6$. The volume fraction is set to $\alpha = 0.0775$ (1 droplet of diameter d), so that $\kappa_d = 2\pi/d - 3$. Top panels show the temporal evolution of the interface during breakup, while vorticity is shown on projected planes. Bottom panels show the surface tension energy transfer function S_σ (see Eq. (2) and Material and Methods) normalized by its maximum values to improve readability. In each plot, in dashed-blue the instantaneous value of S_σ (corresponding to the snapshot above), while the time-averaged value in statistical-stationary condition is reported using a black line. The dotted red line indicates κ_d and time t is normalized with the large-eddies turnover time T_L . The panels show the droplet deformation during the incipient (panel *a* with green background), the sub-critical (panels *b* and *c* with yellow background) and the super-critical (panels *d* and *e* with red background) states. The corresponding video is provided with the Supplementary Movie 1.

important. This is thought to be due to the vorticity creation related to interfaces, which seems to be a crucial feature of intermittency for all practical applications³⁸.

We are now in the position to provide a statistical description which relates intermittency to the Hinze scale. The rationale underlying Eq. (1) is the competition between capillary forces and the turbulent stresses, which are related to the average turbulent dissipation rate. As shown by the refined-Kolmogorov theory $K62$ ^{31,32,39,40}, high-energy intermittent events are occurring within the dissipation range, i.e., localized at small scales⁴¹. The correlation (not necessarily causality) between small droplets and high values of ε , typical of small scales, suggests that a reinterpretation of the breakup theory could be obtained by defining a local random variable ε_ℓ as the integral over a sphere of diameter ℓ of the dissipation field $\varepsilon(\mathbf{x}, t)$. To include intermittency in the picture, we might relate the turbulent forces to the local dissipation rate ε_ℓ at the relevant scale ℓ ; this is in line with Hinze proposition, and introduces a clear scale-dependence in the formula. In this framework, the local dissipation could be estimated as $(\varepsilon_\ell \ell) \sim u_\ell^3$, which should read $\varepsilon_\ell \sim \Pi_\ell$ in a single-phase flow. However, in a multiphase flow at high concentration, the relevant observable for the deformation is precisely the local flux Π_ℓ , which should balance the local dissipation and the interfacial term, so that one should use Π_ℓ rather than ε_ℓ in eq. (1). Hence, if κ_{S_σ} is the wavenumber corresponding to $S_\sigma = 0$ in the shell-by-shell energy budget, the energy flux $\Pi(\kappa_{S_\sigma}) = \sum_0^{\kappa_{S_\sigma}} T(\kappa)$ can be associated with the scale-local velocity fluctuations at the Hinze scale. By replacing ε with $\Pi(\kappa_{S_\sigma})$ in (1) we obtain a refined definition of the Hinze scale:

$$d_H^r = \left(\frac{\rho_c}{\sigma}\right)^{-3/5} \Pi(\kappa_{S_\sigma})^{-2/5}. \quad (4)$$

Note that our modified picture reduces to the original Hinze prediction at low volume fractions when turbulence modulation is negligible, consistently with the hypothesis discussed in ref. 19, as $\Pi_\ell \sim \varepsilon_\ell \sim \langle \varepsilon \rangle$ and the surface tension energy flux is vanishing. The prediction obtained from this relation are compared to classic KH theory in Fig. 4. Most of the values of d_H^r from Eq. (4) coincide with the values of $d_{H\sigma} = 2\pi/\kappa_{S_\sigma}$ when using a pre-factor

0.8, clearly improving over the standard definition in Eq. (1). The pre-factor is most likely accounting for finite- Re_λ effects. It is important to stress that the lack of the empirical parameter We_c in the model proposed in Eq. (4) (unlike in Eq. (1)) suggests that the main factor contributing to the variability of We_c observed in literature is the scale-by-scale energy transport modulation introduced by the dispersed phase. As a final remark, we note that Eq. (4) assumes a clear scale separation between the forcing and the dissipation, so that the nonlinear flux is not negative at the Hinze scale.

Discussion

In the present study, we provide evidences for two crucial hypothesis on the dynamics of multiphase flows when turbulence modulation by the dispersed phase cannot be neglected. First, we propose an unambiguous definition of the Hinze scale based on the analysis of the scale-by-scale energy transfer: this is the scale where the net energy transferred by the interfacial forces is zero. This scale separates two regimes: the dynamics at large scales ($d > d_H$) is characterized by a local fragmentation cascade and a net loss of energy of the larger flow structures when interacting with the dispersed phase. Droplet coalescence and interfacial deformations, instead, dominate at smaller scales where energy is re-injected as a result of a non-local process, further extending the dissipative range toward smaller scales³⁶. Secondly, we demonstrate the link between the droplet size distribution, with pivoting Hinze scale, and the turbulent intermittency. Intermittent rare events at small scale increase in the presence of droplets, with a probability proportional to $d^{13/2} \mathcal{N}(d)$. In addition, we show that a consistent new definition of the Hinze scale can be achieved considering local intermittent fluctuations of the dissipation in the spirit of the Kolmogorov refined similarity hypothesis.

Although energy fluxes are difficult to measure, the scale $d_H^r = (\rho_c/\sigma)^{-3/5} \Pi(\kappa_{S_\sigma})^{-2/5}$ does not depend on any fitting parameter. As $d_H^r \approx d_{H\sigma}$, this scale can be estimated from measurements of the droplet-size spectrum and it can be used to estimate the local energy flux $\Pi(\kappa_{S_\sigma})$. Knowing $\langle \varepsilon \rangle$, one can obtain $\Pi^\sigma(\kappa_{S_\sigma}) = \sum_0^{\kappa_{S_\sigma}} S_\sigma = \langle \varepsilon \rangle - \Pi(\kappa_{S_\sigma})$, which is the energy net flux across the wavenumber κ_{S_σ} due to surface tension forces, i.e., the

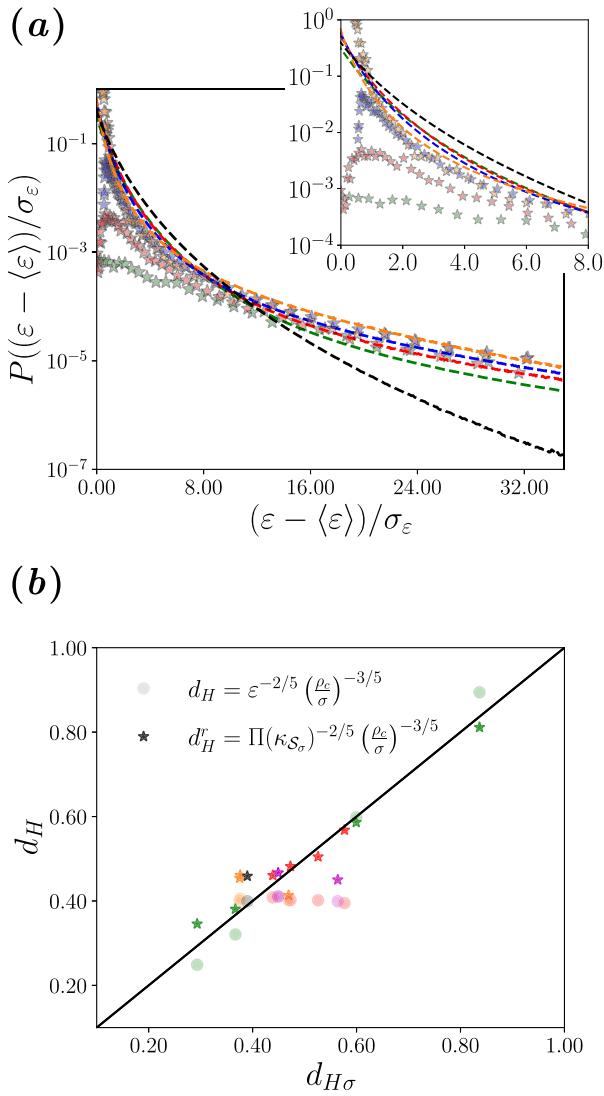


Fig. 4 Revisiting the KH scale, through scale-local energy fluxes. **a** Probability-density-function for the normalized energy dissipation rate ϵ . Black dashed line is the reference single-phase case and colored dashed lines show data from multiphase simulations at different volume fractions α , i.e., 0.03 (green dashed line) 0.06 (red dashed line) 0.1 (blue dashed line) 0.5 (ocher dashed line) at constant large-scale Weber number (see Methods) $We_L = 42.6$ and $\mu_d/\mu_c = 1$. The stars indicate the values of epsilon computed from the DSD where $\epsilon \propto d^{-5/2}$ and $P(\epsilon) \propto d^{13/2}N(d)$ and their color indicates the case (same coloring as dashed lines). The inset shows the details for the PDF at low ϵ . **b** Comparison among the different methods used to compute the Hinze scale, i.e., the original formulation d_H , and the proposed approach d_{H^r} , obtained as the scale at which $S_\sigma = 0$. For d_H , we show two formulations, namely the original formulation proposed in¹⁹ (circles), and the novel interpretation d_H^r (stars). The computation of d_H^r uses the wavenumber-local non-linear fluxes at $\Pi(\kappa_{S_\sigma})$, with $\kappa_{S_\sigma} = 2\pi/d_{H^r}$. The pre-factor 0.8 is used in the expression of d_H^r , to account for finite Re_λ effects. The black diagonal line shows where $d_H^r = d_H$, highlighting the improvement provided by the novel interpretation of the Hinze scale. Colors indicates different α (red) at $We_L = 42.6$ and $\mu_d/\mu_c = 1$; different We_L (green) at $\mu_d/\mu_c = 1$ and $\alpha = 0.03$; different μ_d/μ_c (purple) at $\alpha = 0.1$ and $We_L = 42.6$, and different μ_d/μ_c (yellow) at $\alpha = 0.03$ and $We_L = 42.6$.

Table 1 Parameter settings for the simulations considered in this study: viscosity ratio μ_d/μ_c , Weber number We_L with surface tension σ , volume fraction α and integration time to reach statistical convergence N_T .

	μ_d/μ_c	We_L	σ	α	N_T
SP2	-	-	-	-	136
BE1	1	42.6	0.46	0.03	115
BE2	1	42.6	0.46	0.1	100
V11	0.01	42.6	0.46	0.03	115
V12	0.1	42.6	0.46	0.03	100
V13	10	42.6	0.46	0.03	64
V14	100	42.6	0.46	0.03	60
V21	0.01	42.6	0.46	0.1	115
V22	0.1	42.6	0.46	0.1	100
V23	10	42.6	0.46	0.1	64
V24	100	42.6	0.46	0.1	60
C12	1	42.6	0.46	0.06	100
C13	1	42.6	0.46	0.0775	100
C14	1	42.6	0.46	0.5	100
W11	1	10.6	1.84	0.03	160
W12	1	21.2	0.92	0.03	160
W13	1	106.5	0.184	0.03	100

All simulations are performed with $\mu_c = 0.006$ and same ABC forcing using $N = 512$ grid point in each direction. Each case is denoted by a letter indicating the parameter which is varied: V for viscosity ratio, C volume fraction and W Weber number. SP are the single-phase flows and BE are configurations which recur in different parameterizations (base emulsions). For the single-phase case, the energy dissipation rate is $\epsilon \approx 1.4[L^2][T^{-3}]$, resulting in $n_{sp} = (\nu^3/\epsilon)^{1/4} \approx 2\delta x$. The dissipation is approximately constant in all conditions.

maximum value of Π^σ (see Fig. 2). This computation provides a direct quantification of turbulence modulation due to interfacial forces in multiphase flows. Finally, we stress that, based on our results, from the sole observation of the droplet/bubble size-distribution, one could infer $\langle \epsilon \rangle$ and the dissipation fluctuations (see Fig. 4), hence the most relevant features of the flow.

Dynamical observation of the breaking of a single droplet nicely confirms the statistical picture from a pure geometrical/energetic point of view. We have thus demonstrated that a droplet of size $d = 2\pi/\kappa$ influences the energy transfer at κ through its next topological transformation. In particular, for sub-Hinze inclusions, $d < d_H^r$, we find energy injection associated to creation of small-scale vorticity, whereas we document energy absorption for super-Hinze droplets $d > d_H^r$, bound to break up. The present results provide insights for future coarse-graining modelling of droplet/bubbles dynamics at least when buoyancy effects are negligible. The precise role of density ratio will be addressed in future studies, where also the impact of an anisotropic mean-shear forcing will be considered.

Methods

Numerical simulation. We study emulsions in homogeneous and isotropic turbulence by means of DNS. The problem is described by the one-fluid formulation of the multiphase Navier-Stokes equation:

$$\rho(\partial_t u_i + u_j \partial_j u_i) = -\partial_i p + \partial_i [\mu(\partial_j u_i + \partial_j u_i)] + f_i^\sigma + f_i^T, \tag{5}$$

where u_i is the velocity field, p is the pressure, μ is the flow viscosity, and ρ the fluid density. The term $f_i^\sigma = \sigma \xi \delta_\xi n_i$ represents the surface tension forces, where δ_ξ is a Dirac delta function that concentrate the term action at the surface, with ξ and n_i the interface curvature and normal vector. The term f_i^T is the large scale forcing, used to sustain turbulence throughout the simulation box of size $L = 2\pi$. The forcing is the Arnold-Beltrami-Childress (ABC)^{42,43}, implemented as:

$$f_x^T = A \sin \kappa_0 z + C \cos \kappa_0 y \tag{6}$$

$$f_y^T = B \sin \kappa_0 x + A \cos \kappa_0 z \tag{7}$$

$$f_z^T = C \sin \kappa_0 y + B \cos \kappa_0 x. \tag{8}$$

In order to avoid large-scale coalescence effects, turbulence is forced at $k_0 = 2\pi/\mathcal{L}$, where \mathcal{L} is the injection scale. For all cases presented, $A = B = C = 1$.

The algorithm used to solve Eq. (5) is described in ref. ⁴⁴, while further details on the direct FFT solver used to solve the pressure Poisson equation are provided in ref. ⁴⁵. The interface is captured with the algebraic Volume of Fluid method MTHINC from ⁴⁶.

Case setup. The cases discussed in this work are presented in Table 1. All simulations are performed on a box domain of size 2π , with turbulence forced at $k_0 = 2$ in order to avoid coalescence induced by the large scale dynamics³⁷. The simulation box is discretized with 512³ grid points (see grid-convergence analysis in ref. ³⁶). The total simulation time reported in the table is quantified in terms of large-eddy turnover times, $N_T = t_{\text{tot}}/\mathcal{T}_L$, with $\mathcal{T}_L = \mathcal{L}u_{rms}$ (see ref. ⁴³), where u_{rms} is the velocity fluctuation root-mean-square value. The dispersed phase is initialized on a fully-developed single-phase turbulent field at Taylor-scale Reynolds number $Re_\lambda = 137$. We explore different large-scale Weber number, the ratio between inertial and surface tension forces (i.e., the disperse phase deformability), defined as $We_L = \rho_c \mathcal{L} u_{rms}^2 / \sigma$. Furthermore, we vary the viscosity ratio $\mu_d = \mu_c$ (with d and c being the dispersed and carrier phase) and the dispersed phase volume fraction α . For all simulations, $\rho_d = \rho_c = 1$.

Shell-by-shell energy balance. Significant insight on the flow dynamics is given by the shell-by-shell energy balance. This enables us to quantify the contribution of each term of Eq. (5) to the energy at each scale ℓ , or wavenumber κ in Fourier space. To derive Eq. (2) in the main text, we first perform the Fourier transform (indicated through the symbol $\tilde{\cdot}$) of Eq. (5), yielding

$$\partial_t \tilde{u}_i + \tilde{G}_i = -i\kappa \tilde{p}/\rho - \tilde{V}_i + \tilde{f}_i^\sigma + \tilde{f}_i^T, \quad (9)$$

where \tilde{G}_i and \tilde{V}_i are the Fourier transforms of the non-linear and viscous terms, and i is the imaginary unit. To obtain the energy equation, we multiply Eq. (5) by \tilde{u}_i and repeat the same operations for the complex conjugate velocity and sum the two equations. The resulting terms are $E = \tilde{u}_i \tilde{u}_i^*$ (the kinetic energy in the Fourier space), $T = -(\tilde{G}_i \tilde{u}_i^* + \tilde{G}_i^* \tilde{u}_i)$ (the energy transfer due to the non-linear term), $D = -(\tilde{V}_i \tilde{u}_i^* + \tilde{V}_i^* \tilde{u}_i)$ (the viscous dissipation), $S_\sigma = (\tilde{f}_i^\sigma \tilde{u}_i^* + \tilde{f}_i^{\sigma*} \tilde{u}_i)$ (the work of the surface tension force) and $\mathcal{F} = (\tilde{f}_i^T \tilde{u}_i^* + \tilde{f}_i^{T*} \tilde{u}_i)$ (the energy input due to the large-scale forcing). We finally obtain Eq. (2) by performing a shell-integral, e.g., for the surface tension term $\tilde{S}_\sigma(\kappa) = \sum_{\kappa' < |\kappa|, |\kappa'+1} \tilde{S}_\sigma(\kappa')$. Further details on the derivation and properties of this equation can be found in refs. ^{32,36,47}.

Data availability

All relevant data presented in this paper are available from the corresponding author upon reasonable request.

Code availability

The code used to perform this study is open-source and available at <https://github.com/Multiphysics-Flow-Solvers/FluTAS>.

Received: 25 May 2022; Accepted: 15 December 2022;

Published online: 06 January 2023

References

- Villermaux, E. & Bossa, B. Single-drop fragmentation determines size distribution of raindrops. *Nat. Phys.* **5**, 697–702 (2009).
- Keshavarz, B., Houze, E. C., Moore, J. R., Koerner, M. R. & McKinley, G. H. Ligament Mediated Fragmentation of Viscoelastic Liquids. *Phys. Rev. Lett.* **117**, 154502 (2016).
- Villermaux, E. Fragmentation versus cohesion. *J. Fluid Mech.* **898**, P1 (2020).
- Perlekar, P., Benzi, R., Clercx, H. J., Nelson, D. R. & Toschi, F. Spinodal decomposition in homogeneous and isotropic turbulence. *Phys. Rev. Lett.* **112**, 1–5 (2014).
- Giroto, I., Benzi, R., Di Staso, G., Scagliarini, A., Schifano, S. F., & Toschi, F. Build up of yield stress fluids via chaotic emulsification. *J. Turbulence* **23**, 1–11 (2022).
- Bakhuizen, D. et al. Catastrophic Phase Inversion in High-Reynolds-Number Turbulent Taylor-Couette Flow. *Phys. Rev. Lett.* **126**, 64501 (2021).
- Garrett, C., Li, M. & Farmer, D. The connection between bubble size spectra and energy dissipation rates in the upper ocean. *J. Phys. Oceanogr.* **30**, 2163–2171 (2000).
- Gao, Q., Deane, G. B. & Shen, L. Bubble production by air filament and cavity breakup in plunging breaking wave crests. *J. Fluid Mech.* **929**, A44 (2021).
- Deike, L. Mass Transfer at the Ocean-Atmosphere Interface: The Role of Wave Breaking, Droplets, and Bubbles. *Ann. Rev. Fluid Mech.* **54**, 191–224 (2022).
- Berny, A., Popinet, S., Séon, T. & Deike, L. Statistics of Jet Drop Production. *Geophys. Res. Lett.* **48**, 1–14 (2021).
- Jiang, X., Rotily, L., Villermaux, E. & Wang, X. Submicron drops from flapping bursting bubbles. *Proc. Natl Acad. Sci.* **119**, e2112924119 (2022).
- Skartlien, R., Sollum, E. & Schumann, H. Droplet size distributions in turbulent emulsions: Breakup criteria and surfactant effects from direct numerical simulations. *J. Chem. Phys.* **139**, 174901 (2013).
- Yu, X., Hendrickson, K. & Yue, D. K. Scale separation and dependence of entrainment bubble-size distribution in free-surface turbulence. *J. Fluid Mech.* **885**, R2 (2019).
- Mukherjee, S. et al. Droplet-Turbulence interactions and quasi-equilibrium dynamics in turbulent emulsions. *J. Fluid Mech.* **878**, 221–276 (2019).
- Perrard, S., Rivière, A., Mostert, W. & Deike, L. Bubble deformation by a turbulent flow. *J. Fluid Mech.* **920**, A15 (2021).
- Rivière, A., Mostert, W., Perrard, S. & Deike, L. Sub-Hinze scale bubble production in turbulent bubble break-up. *J. Fluid Mech.* **917**, A40 (2021).
- Yi, L., Toschi, F. & Sun, C. Global and local statistics in turbulent emulsions. *J. Fluid Mech.* **912**, A13 (2021).
- Kolmogorov, A. On the breakage of drops in a turbulent flow. *Dokl. Akad. Nauk. SSSR* **66**, 825–828 (1949).
- Hinze, J. O. Fundamentals of the hydrodynamic mechanism of splitting in dispersion processes. *AIChE J.* **1**, 289–295 (1955).
- Qi, Y. et al. Fragmentation in turbulence by small eddies. *Nat. Commun.* **13**, 1–8 (2022).
- Fuster, D. & Rossi, M. Vortex-interface interactions in two-dimensional flows. *Int. J. Multiphase Flow* **143**, 103757 (2021).
- Kolmogorov, A. N. The Local Structure of Turbulence in Incompressible Viscous Fluid for Very Large Reynolds Numbers. *Proc. Royal Soc. A: Mathem. Phys. Eng. Sci.* **434**, 9–13 (1991).
- Deane, G. B. & Stokes, M. D. Scale dependence of bubble creation mechanisms in breaking waves. *Nature* **418**, 839–844 (2002).
- Blenkinsopp, C. E. & Chaplin, J. R. Bubble size measurements in breaking waves using optical fiber phase detection probes. *IEEE J. Oceanic Eng.* **35**, 388–401 (2010).
- Wang, Z., Yang, J. & Stern, F. High-fidelity simulations of bubble, droplet and spray formation in breaking waves. *J. Fluid Mech.* **792**, 307–327 (2016).
- Chan, W. H. R., Johnson, P. L., Moin, P. & Urzay, J. The turbulent bubble break-up cascade. Part 2. Numerical simulations of breaking waves. *J. Fluid Mech.* **912**, A43 (2021).
- Li, C., Miller, J., Wang, J., Koley, S. & Katz, J. Size distribution and dispersion of droplets generated by impingement of breaking waves on oil slicks. *J. Geophys. Res.: Oceans* **122**, 7938–7957 (2017).
- MARTÍNEZ-BAZÁN, C., Montanes, J. & Lasheras, J. C. On the breakup of an air bubble injected into a fully developed turbulent flow. part 1. breakup frequency. *J. Fluid Mech.* **401**, 157–182 (1999).
- Benzi, R., Paladin, G., Parisi, G. & Vulpiani, A. On the multifractal nature of fully developed turbulence and chaotic systems. *J. Phys. A: Mathematical General* **17**, 3521 (1984).
- Meneveau, C. & Sreenivasan, K. Simple multifractal cascade model for fully developed turbulence. *Phys. Rev. Lett.* **59**, 1424 (1987).
- Boffetta, G., Mazzino, A. & Vulpiani, A. Twenty-five years of multifractals in fully developed turbulence: A tribute to Giovanni Paladin. *J. Phys. A: Mathematical Theor.* **41** (2008).
- Frisch, U. *Turbulence* (Cambridge University Press, 1995). <https://www.cambridge.org/highereducation/books/turbulence/FD8C5E35E5F1CA850E017461942A59AC#contents>.
- Pope, S. *Turbulent Flows* (Cambridge University Press, 2009), sixth edn.
- Alexakis, A. & Biferale, L. Cascades and transitions in turbulent flows. *Phys. Rep.* **767**, 1–101 (2018).
- Rivière, A., Ruth, D. J., Mostert, W., Deike, L., & Perrard, S. Capillary driven fragmentation of large gas bubbles in turbulence. *Phys. Rev. Fluid* **7**, 083602 (2022).
- Crialesi-Esposito, M., Rosti, M. E., Chibbaro, S. & Brandt, L. Modulation of homogeneous and isotropic turbulence in emulsions. *J. Fluid Mech.* **940**, A19 (2022).
- Komrakova, A. E., Eskin, D. & Derksen, J. J. Numerical study of turbulent liquid-liquid dispersions. *AIChE J.* **61**, 2618–2633 (2015).
- Buaria, D. & Pumir, A. Vorticity-strain rate dynamics and the smallest scales of turbulence. *Phys. Rev. Lett.* **128**, 094501 (2022).
- Kolmogorov, A. N. A refinement of previous hypotheses concerning the local structure of turbulence in a viscous incompressible fluid at high Reynolds number. *J. Fluid Mech.* **13**, 82–85 (1962).
- Dubrulle, B. Beyond Kolmogorov cascades. *J. Fluid Mech.* **867**, P1 (2019).

41. Buzzicotti, M., Biferale, L. & Toschi, F. Statistical properties of turbulence in the presence of a smart small-scale control. *Phys. Rev. Lett.* **124**, 084504 (2020).
42. Podvigina, O. & Pouquet, A. On the non-linear stability of the 1:1:1 ABC flow. *Phys. D: Nonlinear Phenomena* **75**, 471–508 (1994).
43. Mininni, P. D., Alexakis, A. & Pouquet, A. Large-scale flow effects, energy transfer, and self-similarity on turbulence. *Phys. Rev. E - Statistical, Nonlinear, Soft Matter Phys.* **74**, 1–13 (2006).
44. Rosti, M. E., Ge, Z., Jain, S. S., Dodd, M. S. & Brandt, L. Droplets in homogeneous shear turbulence. *J. Fluid Mech* **876**, 962–984 (2020).
45. Costa, P. A FFT-based finite-difference solver for massively-parallel direct numerical simulations of turbulent flows. *Comput. Mathem. Appl.* **76**, 1853–1862 (2018).
46. Li, S. et al. An interface capturing method with a continuous function: The THINC method with multi-dimensional reconstruction. *J. Comput. Phys.* **231**, 2328–2358 (2012).
47. Alexakis, A. & Biferale, L. Cascades and transitions in turbulent flows. *Phys. Rep.* **767-769**, 1–101 (2018).

Acknowledgements

This work was supported by the Swedish Research Council via the multidisciplinary research environment INTERFACE, Hybrid multiscale modelling of transport phenomena for energy efficient processes, Grant no. 2016-06119. The authors acknowledge computer time provided by the National Infrastructure for High Performance Computing and Data Storage in Norway (Sigma2, project no. NN9561K) and by SNIC (Swedish National Infrastructure for Computing).

Author contributions

M.C.E., S.C., and L.B. conceived the research. M.C.E. performed the numerical simulations and the statistical analysis. All authors wrote the paper and contributed to the physical interpretations.

Funding

Open access funding provided by Royal Institute of Technology.

Competing interests

The authors declare no competing interests.

Additional information

Supplementary information The online version contains supplementary material available at <https://doi.org/10.1038/s42005-022-01122-8>.

Correspondence and requests for materials should be addressed to Marco Cialesi-Esposito, Sergio Chibbaro or Luca Brandt.

Peer review information *Communication Physics* thanks the anonymous reviewers for their contribution to the peer review of this work.

Reprints and permission information is available at <http://www.nature.com/reprints>

Publisher's note Springer Nature remains neutral with regard to jurisdictional claims in published maps and institutional affiliations.



Open Access This article is licensed under a Creative Commons Attribution 4.0 International License, which permits use, sharing, adaptation, distribution and reproduction in any medium or format, as long as you give appropriate credit to the original author(s) and the source, provide a link to the Creative Commons license, and indicate if changes were made. The images or other third party material in this article are included in the article's Creative Commons license, unless indicated otherwise in a credit line to the material. If material is not included in the article's Creative Commons license and your intended use is not permitted by statutory regulation or exceeds the permitted use, you will need to obtain permission directly from the copyright holder. To view a copy of this license, visit <http://creativecommons.org/licenses/by/4.0/>.

© The Author(s) 2023